ELSEVIER

Journal of the Neurological Sciences 164 (1999) 29–36

Journal of the Neurological Sciences

Dynamic changes in glucose metabolism induced by thiamine deficiency and its replenishment as revealed by a positron autoradiography technique using rat living brain slices

Tetsuhito Murata[a,b,*], Naoto Omata[a], Yasuhisa Fujibayashi[a], Atsuo Waki[a], Norihiro Sadato[a], Mitsuyoshi Yoshimoto[a], Masao Omori[b], Kiminori Isaki[b], Yoshiharu Yonekura[a]

[a]*Biomedical Imaging Research Center, Fukui Medical University, Matsuoka-cho, Fukui 910-1193, Japan*
[b]*Department of Neuropsychiatry, Fukui Medical University, Matsuoka-cho, Fukui 910-1193, Japan*

Received 28 May 1998; received in revised form 2 February 1999; accepted 10 February 1999

Abstract

Dynamic changes in the cerebral glucose metabolic rate (CMRglc) before and after thiamine replenishment were investigated in living brain slices obtained from pyrithiamine-treated (PT) and pair-fed control rats by use of a positron autoradiography technique. Fresh rat brain slices (300 μm thick) were incubated with [^{18}F]2-fluoro-2-deoxy-D-glucose ([^{18}F]FDG) in oxygenated Krebs–Ringer solution at 36°C, during which serial two-dimensional images of [^{18}F]FDG uptake in the slices were constructed on the imaging plates. The net influx constant (=K) of [^{18}F]FDG was determined by a Patlak graphical method of the image data. Prior to thiamine pyrophosphate (TPP)-loading, the K value in the neurologically symptomatic PT was higher in all brain regions except the thalamus and mammillary body than the control, suggesting compensatory enhanced glycolysis. The rapid decrease in this heightened net influx constant immediately after TPP-loading was surmised to be due to activation of pyruvate oxidation with lactate as the substrate, with this inhibiting the glycolysis. From ≥150 min after TPP-loading, the K value continued to show low values in the thalamus and mammillary body, which are regarded as the responsible sites for Korsakoff syndrome, whereas in all other sites recovery to control values was observed. These findings suggest that using this technique the quantitative evaluation of serial local changes in CMRglc from thiamine deficiency to after its replenishment may be useful in elucidating the pathophysiology and prognosis of Wernicke's encephalopathy.

Keywords: Brain slice; Thiamine; Wernicke's encephalopathy; Glucose metabolism; [^{18}F]FDG; Korsakoff syndrome; Positron

1. Introduction

Wernicke's encephalopathy which results from a deficiency of thiamine (vitamin B1), shows the three classical signs of progressive unconsciousness, ataxia and ophthalmoplegia [1], and is characterized by specific lesions localized to parts of the brain such as the thalamus, mammillary body and periventricular regions [2,3]. Administration of pyrithiamine provides an adequate pathological model of thiamine deficiency [4,5] and is known to suppress the activities of the same enzymes that are affected by dietary deprivation of thiamine [6,7], namely, pyruvate dehydrogenase complex (PDHC), alpha-ketoglutarate dehydrogenase (αKGDH), and transketolase (TK). These enzymatic steps affected by thiamine deficiency are intimately involved in glucose metabolism. When thiamine is replenished in the early period good recovery can be anticipated [8,9]; otherwise severe and irreversible brain damage such as Korsakoff syndrome may persist [1,10]. To search for indices that can serve as clues to the threshold of reversibility with treatment and pathophysiology of Wernicke's encephalopathy, further studies on serial changes in glucose utilization from

*Corresponding author. Tel.: +81-776-61-3111, ext. 2335; fax: +81-776-61-8137.

0022-510X/99/$ – see front matter
PII: S0022-510X(99)00055-6

thiamine deficiency until after its replenishment are being awaited.

Measurement of the cerebral glucose metabolic rate (CMRglc) using 2-deoxyglucose (2DG) and the tracer kinetic model of Sokoloff et al. [11] has become a fundamental method to assess brain function. Hitherto, quantitative studies with meticulous tracer kinetic modeling with application of the [^{14}C]2DG method to living brain slices have been proposed by Newman et al. [12]. In these studies the amount of radioactivity uptake to the tissue is counted either with a liquid scintillation counter or by image analysis after autoradiography, only at a defined time point for sampling after removing the free radiotracer surrounding the tissue. We recently established an imaging technique in living brain slices, named 'dynamic positron autoradiography technique' (dPAT), utilizing positron emitter-labeled ligands as a probe and an imaging plate as a detector [13,14]. Due to the high specific radioactivity of the radiotracers, high energy of beta particles, and high sensitivity of the imaging plate, serial two-dimensional images of radioactivity in the slices can be constructed quantitatively with a short exposure time, while the brain tissue is still alive in the incubation solution.

The purpose of the present study was to investigate the dynamic changes in regional CMRglc from thiamine deficiency until after its replenishment. Using the dPAT technique with [^{18}F]2-fluoro-2-deoxy-D-glucose ([^{18}F]FDG) and fresh brain slices obtained from the pyrithiamine-treated (PT) and pair-fed control rats, we quantitatively analyzed serial changes in the regional net influx constant of [^{18}F]FDG when thiamine pyrophosphate (TPP) was exogenously loaded in the bathing medium.

2. Materials and methods

2.1. Experimental procedure and treatment groups

Male Sprague-Dawley rats weighing 250–300 g were used for the experiments. PT rats were fed the thiamine-deficient diet and given daily injections of pyrithiamine (50 μg/100 g body weight, i.p.). Neurological status was evaluated daily by observing their spontaneous movements and gait, and the following treatment groups were used for the experiments; (1): PT presymptomatic at which rats showed no evidence of neurological abnormalities of gait or righting reflex. Experiments were conducted on the 12–13th day after the initiation of pyrithiamine administration. (2): PT symptomatic at which rats showed neurological deficits. This stage was reached by the 14–16th day. In almost all cases ataxic gait, loss of righting reflex and opisthotonus were noted, with convulsions also developing in a few cases. The rats were used for the experiments within 20 h after these neurological symptoms were observed. The experiments were conducted on a total of 16 animals consisting of 4 each from the above-mentioned (1) and (2) and 4 pair-fed control rats each. These control rats were pair-fed a thiamine-deficient diet equal to the food consumption of PT rats and received daily injections of thiamine (10 μg/100 g body weight, i.p.) up to the day of the experiment.

The blood thiamine concentration was measured in all of the rats on the day that they were supplied for the experiments. The measured values in PT rats (pre-symptomatic group: 38±11 ng/ml, symptomatic group: 21±6 ng/ml) were decreased to less than 5–10% of the respective values in the pair-fed control group (405±61 ng/ml, 452±94 ng/ml). All group rats were weighed every day. PT rats gained weight for approximately the first 10 days of the experiment, the average weight gain during this period being 30% over the starting weight. This was followed by gradual weight loss, resulting in the weight at sacrifice of the PT symptomatic rats being about 10% less than the starting value.

2.2. Preparation of brain slices and setup for incubation

PT rats and their corresponding pair-fed controls were anesthetized with diethyl ether. After decapitation, the brains were quickly removed and immersed in oxygenated and cooled (1–4°C) Krebs-Ringer solution (having the following composition in mM concentrations: NaCl, 124; KCl, 5; $MgCl_2$, 1; $CaCl_2$, 2; KH_2PO_4, 1.2; $NaHCO_3$, 26; glucose, 10). Brain slices of 300 μm thickness were prepared with a microslicer (DTK-2000; Dosaka EM, Kyoto, Japan). The slices were incubated in double polystyrene chambers (outer and inner ones) as described previously [14]. Their side view is illustrated in Fig. 1A. Briefly, the bottom of both the outer and inner chambers was cut to make a rectangular hole, over which a transparent polyvinylidene chloride film (10 μm thick) or a fine nylon net (80 μm thick) was tightly stretched and fixed in place by gluing it to the side wall, respectively. The outer chamber was filled with 80 ml of Krebs–Ringer solution, in which the inner chamber having numerous small holes (4 mm in diameter) on the side wall was immersed. Brain slices were arranged on the nylon net of the inner chamber and were lightly fixed in place by covering them with a fine nylon net, which was stretched and glued to the upper side of a 300 μm thick stainless steel ring (2 cm in inner diameter). On macroscopic observation of the cut out slices no abnormalities were noted with the exception of punctate hemorrhages in the thalamus and inferior colliculus in a few cases of the PT symptomatic group. The bathing solution was continuously bubbled with 95% O_2/5% CO_2 gas supplied through fine silicone tubing introduced into the inner chamber at six sites, to promote consistent perfusion within the chamber.

2.3. Production of radiotracer and measurement of [^{18}F]FDG uptake

^{18}F was produced by ^{18}O(p,n) ^{18}F nuclear reaction, and [^{18}F]FDG was synthesized by the method of Hamacher et

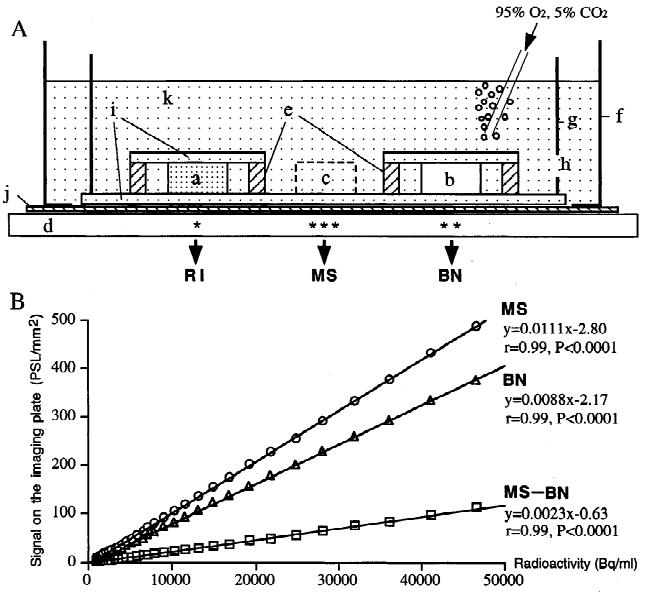

Fig. 1. (A): Schematic side view of the setup for incubation and radioactivity signal detected on the imaging plate. *a*, brain slice (300 μm thick); *b*, nylon sheet (300 μm thick); *c*, 300-μm-thick bathing solution layer; *d*, imaging plate; *e*, stainless steel ring; *f*, outer chamber; *g*, inner chamber; *h*, hole on the side wall of the inner chamber; *i*, nylon net (80 μm thick); *j*, polypropylene sheet (10 μm thick); *k*, Krebs-Ringer solution containing [^{18}F]FDG. For simplification, the scaling is arbitrary. (B): Linear relationship between the response of the imaging plates (PSL/mm^2) to the radioactivity (Bq/ml) in the cases of MS (***), BN (**), and MS minus BN. In all three, regression lines passing close to the original points could be fitted, with all the data presented here within the linear range.

al. [15] with an automated [^{18}F]FDG synthesis system (NKK Co. Ltd., Tokyo, Japan). The specific radioactivity of [^{18}F]FDG was 1–2 Ci/mmol at the end of synthesis, with the total concentration (labeled plus unlabeled) used in this study ranging from 0.41 to 1.17 μg/ml (2.4–6.9 μM). After 1 h preincubation of brain slices in Krebs–Ringer solution at 36°C (pH 7.3–7.4), the inner chamber containing the slices was taken out and put into another outer chamber in which [^{18}F]FDG had been diluted at 150 kBq/ml with prewarmed Krebs–Ringer solution. A set of four double chambers, each of which contained eight slices (cut out of each individual rat), were put on an imaging plate (BAS-MP 2040S, Fuji Photo Film Co., Tokyo, Japan), which was replaced with a new plate every 10 min. Exposed imaging plates were scanned with a bio-imaging analyzer (BAS-1500, Fuji Photo Film Co.), and the images were displayed on a Macintosh computer. The pixel size was 100 μm.

2.4. Calculation of CMRglc and Patlak graphical analysis

The three compartment model for [^{18}F]FDG using brain slices is based on the distribution of [^{18}F]FDG in bathing medium [Cp*(t)], [^{18}F]FDG in tissue [Ce*(t)], and [^{18}F]FDG-6-PO$_4$ in tissue [Cm*(t)] [11,12]. First-order rate constants describing the transport between the compartments include K_1^* and k_2^* for forward and reverse [^{18}F]FDG transport, k_3^* and k_4^* for phosphorylation of [^{18}F]FDG and dephosphorylation of [^{18}F]FDG-6-PO$_4$. In the equilibrium condition, as the influx constant of [^{18}F]FDG$=(K_1^*K_3^*)/(k_2^*+k_3^*)$ is equivalent to the rate of [^{18}F]FDG-6-PO$_4$, CMRglc can be estimated with the following expression [16]:

$$\text{CMRglc} = \text{Cp}/\text{LC}\,(K_1^*k_3^*/(k_2^* + k_3^*)) = \text{Cp}/\text{LC} \cdot \text{K} \qquad (1)$$

where Cp is the medium glucose concentration and LC is the lumped constant, which accounts for differences in the transport and phosphorylation of [^{18}F]FDG and glucose [11,16,17]. K is the macroparameter for the net influx constant of [^{18}F]FDG. If both the Cp and LC are constant, the linear relationship should be kept between K and CMRglc according to Eq. 1, and thus K itself can be considered as an index of CMRglc. The Patlak graphical method [18,19] employed to determine the macroparameter K was based on the following equation

$$\text{Ci}^*(t)/\text{Cp}(t) = K \cdot \int_0^t \text{Cp}^*(\tau)\,\text{d}\tau/\text{Cp}^*(t) + V \qquad (2)$$

where Ci*(t), which is equal to the sum of Ce*(t) and Cm*(t), is the total tissue radioactivity, Cp*(t) is the input function, and V is related to the effective distribution volume of the tracer [^{18}F]FDG. Thus, with the assumption that k4* is equal to zero, K was estimated from the slope of the linear portion of the graph, Ci*(t)/Cp*(t) (vertical Y axis) versus $\int_0^t$ Cp*(τ) dτ/Cp*(t) (horizontal X axis).

To perform quantitative analysis based on Patlak graphical method, as a slice phantom, a 300 μm thick nylon sheet (specific gravity = 1.14) ((b) in Fig. 1A) of approximately the same size as the slices was set up under the same experimental conditions as the 300 μm thick brain slices ((a) in Fig. 1A). Then, in the surrounding medium solution as well, 300 μm thick bathing solution was assumed in the same position as this ((c) in Fig. 1A), and the radioactivity signal from each 300 μm thick layer (brain slice, nylon sheet, bathing solution) and the radioactivity signal from the medium solution above and below these layers were divided, with the contribution of each to the radioactivity signal measured on the imaging plate estimated. First, no differences were thought to be present in the radioactivity signal contributed by the medium solution beneath each layer (present in the gaps in the nylon net between each layer and imaging plate). Next, the density of brain tissue, nylon sheet and medium solution was in each case close to one, and since the radioactivity signal from the medium solution above each layer passed through each layer with the same attenuation rate, the radioactivity signal contributed by these was thought to be equal.

Accordingly, when RI is defined as the radioactivity signal (PSL (photostimulated luminescence)/mm^2) on the

imaging plate detected beneath the region of interest ((*) in Fig. 1A), BN as the radioactivity signal on the imaging plate detected beneath the nylon sheet for measuring the background noise ((**) in Fig. 1A), and MS as the average radioactivity signal on the imaging plate detected at four places beneath the bathing medium solution surrounding each brain slice or nylon sheet ((***) in Fig. 1A), the portion of the radioactivity signal contributed only by the 300 μm thick brain tissue can be calculated from RI−BN, and in the same way the portion of the radioactivity signal contributed only by the 300 μm thick bathing solution can be calculated from MS−BN, since the radioactivity signal from the 300 μm thick nylon sheet is zero. Here, the same amount of [^{18}F]FDG either in a 300 μm thick brain slice or in a 300 μm thick bathing solution layer (the densities of which are nearly equal) should yield the same amount of signal on the imaging plate. Thus, $Ci^*(t)/Cp^*(t)$ can be expressed in terms of the following ratio:

$$Ci^*(t)/Cp^*(t) = (RI - BN)/(MS - BN) \quad (3)$$

Here, the linearity of the response of the imaging plates (PSL/mm^2) to the radioactivity (Bq/ml) was checked previously in the cases of BN, MS, and MS−BN (Fig. 1B). In all three, regression lines passing close to the original points could be fitted, with all the data presented here within the linear range respectively. In addition, by comparing the slope of the respective regression lines, if within this linear range, it was suggested that an approximate relation of $BN = 0.8 \times MS$ could be established. In fact, instead of setting up the slice phantom in all of the experiments to calculate BN of Eq. 3, we routinely substituted $0.8 \times MS$ for BN and calculated $Ci^*(t)/Cp^*(t)$.

The real radioactivity signal of MS−BN decreased exponentially as the time passed from the start of incubation, while when decay-corrected it showed an almost constant signal throughout the whole time course (data not presented). Thus, $Ci^*(t)/Cp^*(t)$ (vertical Y axis) at each time point calculated above was plotted against time (horizontal X axis) indicating $\int_0^t Cp^*(\tau)\, d\tau/Cp^*(t)$ based on the Patlak graphical method (as the mean value of 8 slices). Time zero ($t=0$) is when [^{18}F]FDG was introduced into the bathing medium containing brain slices. As shown in Fig. 3 for instance, $Ci^*(t)/Cp^*(t)$ within the initial part (from 0 to 60 min) of each plot did not show a linear relationship with time, indicating non-steady condition between the incubation medium and the slices. After that, the $Ci^*(t)/Cp^*(t)$ of the pair-fed control under unloaded condition showed a linear relationship with time (linear regression coefficient $r>0.98$, from 60 to 380 min), indicating the constant glucose utilization. When TPP-loading was introduced into the bathing medium, it took 20–30 min before reaching a new equilibrium state, with this temporary phase manifested as a transient curve. To evaluate the dynamic changes in the net influx constant of [^{18}F]FDG by TPP-loading, the slope ($=K$) was calculated from a linear portion of the Patlak plot under each equilibrium state in the pre- and post-loading phases separately using the linear regression analysis.

2.5. Determination of lactate levels in brain tissue

Lactate was measured using an enzymatic kit (TC L-Lactic Acid, Boehringer Mannheim Co., Mannheim, Germany), which uses lactate dehydrogenase to convert lactate and NAD^+ to pyruvate and NADH respectively. Two slices per chamber were taken out of the incubation solution, their weight immediately measured after gently removing the adherent water with filter paper, and then the slices were homogenized in 0.2 ml of ice-cold phosphate-buffered saline (pH 7.4). The homogenate was heat-treated (80°C) for 15 min, and centrifuged for 3 min at $15\,000 \times g$. The supernatant (0.1 ml) was used for analysis of lactate. NADH was measured fluorometrically with the excitation at 340 nm and emission at 450 nm using UV-3101PC (Shimadzu Corp., Kyoto, Japan).

2.6. Experimental analysis

Data analysis was performed on a Macintosh computer and the images were analyzed using the software MacBAS version 2 (Fuji Photo Film Co.) developed for Macintosh computers. The presented values are shown as the mean±S.E.M. of a total of eight or sixteen slices obtained from four rats. The Mann-Whitney U test or the one-way ANOVA with post-hoc comparison test were used to evaluate the significance of differences.

3. Results

3.1. PT symptomatic group

Fig. 2 shows time-resolved images of [^{18}F]FDG uptake of two typical slices obtained from the pair-fed control (A) and the PT symptomatic (B) rats in two representative time periods; before (150–160 min) and after (330–340 min) the loading of 1 mM TPP. TPP was introduced into the bathing medium at 170 min. Fig. 3 shows the Patlak plots of the slices from the PT symptomatic and the control group throughout the time course in two representative brain regions: frontal cortex and thalamus. The graph indicates that the slope ($=K$) of the PT symptomatic group was drastically decreased by TPP with a latency of less than 10 min to reach a new equilibrium state, and was reversed in the frontal cortex during the latter time course. Changes in the net influx constant of [^{18}F]FDG in the PT symptomatic group throughout the time course (before and after the application of TPP) are shown in Table 1. The pre-TPP-loading K value as compared to the pair-fed control was larger in the frontal cortex, caudate putamen, hippocampus and cerebellum, and smaller in the thalamus

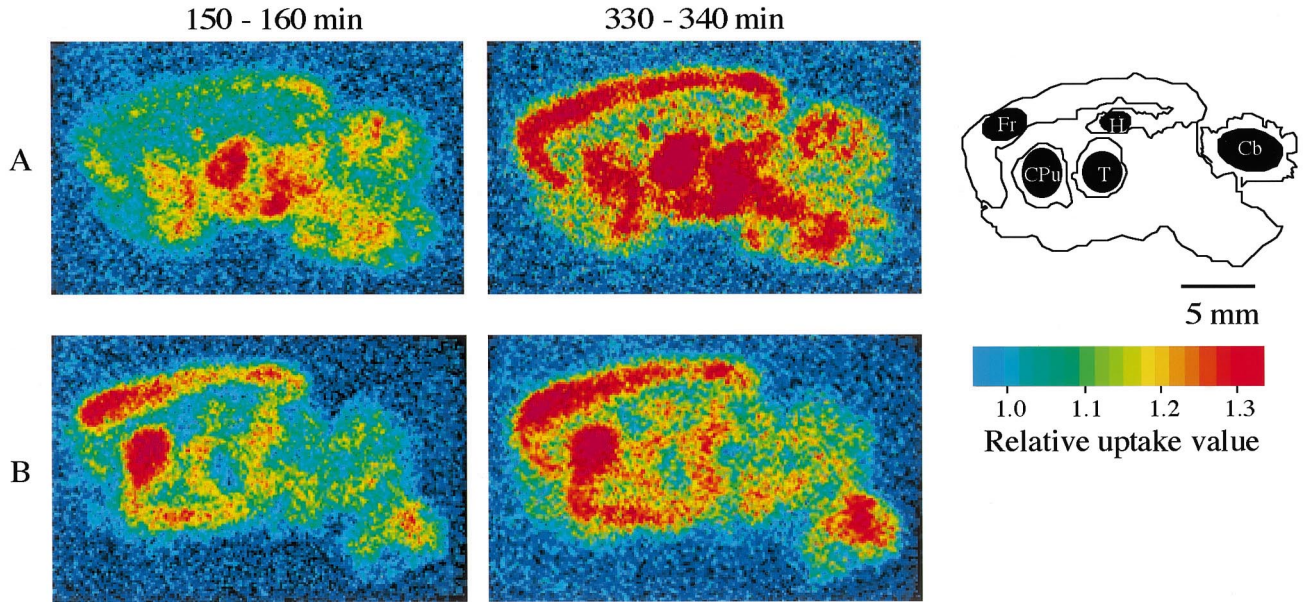

Fig. 2. Time-resolved pseudo-color images of [^{18}F]FDG uptake in sagittally sectioned rat brain slices. Time zero ($t=0$) is when [^{18}F]FDG was introduced into the bathing medium containing brain slices. Two typical slices obtained from the pair-fed control (A) and the PT symptomatic (B) rats focusing on 2 representative time periods: before (150–160 min) and after (330–340 min) the TPP-loading. TPP-loading was introduced into the bathing medium at 170 min. Filled circles in the diagram represent the five brain regions of interest (Fr: frontal cortex, CPu: caudate putamen, T: thalamus, H: hippocampus, Cb: cerebellum). Mammillary bodies not included in slices of the same plane are not displayed. For decay correction, the color-coding was made on the relative uptake value, which was calculated by dividing each pixel value of the slices by the averaged pixel value of the surrounding solution.

and mammillary body. The *K* value after 20–80 min had passed from TPP-loading was markedly lower as compared to the pre-loading and unloaded pair-fed control values in all sites. Moreover, after 150–210 min had passed from TPP-loading recovery to close to pair-fed control group values occurred in the majority of sites, with the thalamus and mammillary body notable exceptions in which recovery was not observed.

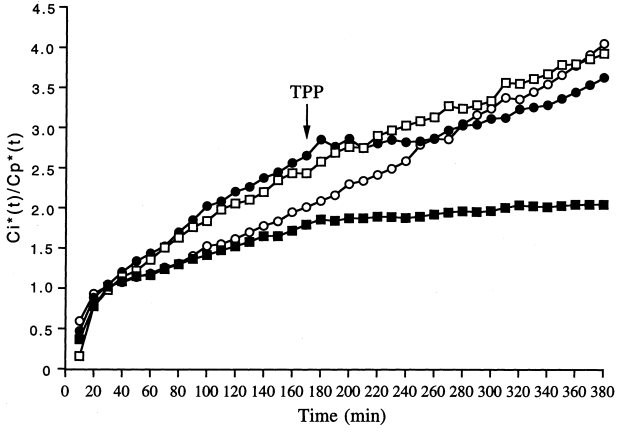

Fig. 3. Effect of 1 mM TPP on the Patlak plots of [^{18}F]FDG uptake in two representative brain regions from the PT symptomatic (closed symbols) and the pair-fed control (open symbols) group; frontal cortex (circles) and thalamus (squares). Addition of TPP is indicated by the arrow. Ordinate: $[C_i^*(t)/C_p^*(t)]$ expressed in terms of the radioactivity signal ratio $(=(RI-BN)/(MS-BN))$ versus Abscissa: time (min) indicating $[\int_0^t C_p^*(\tau)d\tau/C_p^*(t)]$ (see text for further explanation). Time zero is when [^{18}F]FDG was introduced into the bathing medium containing brain slices. Values are means obtained from sixteen slices from four rats (S.E.M. were omitted).

Serial changes in lactate levels in whole brain slices just prior to and after the TPP-loading were calculated as the mean values of 8 slices (2 each per rat). Lactate levels of the PT symptomatic group showed a significant decrease post- as compared to pre-loading (preloading: 2.57±0.33 nmol/mg tissue, 30 min postloading: 1.94±0.27 nmol/mg tissue, $P<0.01$). In contrast, no such change was found in the pair-fed control group (preloading: 2.11±0.22 nmol/mg tissue, 30 min postloading: 2.14±0.21 nmol/mg tissue).

3.2. PT presymptomatic group

The PT presymptomatic group was investigated in the same way as the PT symptomatic group. Changes in the net influx constant of [^{18}F]FDG throughout the time course (before and after the application of TPP) are shown in Table 2. The K value of the PT presymptomatic group throughout the time course showed no difference at any site as compared with the control group.

Similarly, no change in lactate levels just prior to and after the TPP-loading was found in the PT presymptomatic group (preloading: 2.03±0.21 nmol/mg tissue, 30 min postloading: 2.15±0.21 nmol/mg tissue) or in the pair-fed control group (preloading: 1.98±0.22 nmol/mg tissue, 30 min postloading: 2.10±0.21 nmol/mg tissue).

Table 1
Effect of TPP on the net influx constant of [^{18}F]FDG in the PT symptomatic group (PT-SYM) throughout the time course (before and after the application of 1 mM TPP)[a]

Brain region		Before	20–80 min after	150–210 min after
Frontal cortex	Control	6.91±0.66	7.25±0.56	8.13±0.72
	PT-SYM	10.45±1.15[b]	0.73±0.24[b,c]	5.79±1.08[c,d]
Caudate putamen	Control	8.93±1.22	7.76±0.91	6.92±0.52
	PT-SYM	14.45±2.03[b]	0.12±0.17[b,c]	2.40±0.44[b,c,d]
Thalamus	Control	8.27±0.84	7.24±0.70	6.51±0.64
	PT-SYM	5.02±1.08[b]	0.66±0.21[b,c]	0.77±0.40[b,c]
Hippocampus	Control	7.20±0.77	6.35±0.70	7.43±0.64
	PT-SYM	9.55±0.94[b]	0.92±0.24[b,c]	5.65±0.92[c,d]
Mammillary body	Control	6.41±0.98	5.58±1.01	4.38±0.96
	PT-SYM	4.96±0.84[b]	0.55±0.03[b,c]	0.70±0.52[b,c]
Cerebellum	Control	8.72±0.66	7.79±0.74	6.92±0.44
	PT-SYM	11.60±0.84[b]	1.01±0.35[b,c]	3.95±0.88[b,c,d]

[a] The macroparameter $K(\times 1000)$, indicating the net influx constant of [^{18}F]FDG, was obtained from the slope of the regression Eq. ($Y=aX+b$) fitted to Patlak plots using the linear regression analysis Y:[$C_i^*(t)/C_p^*(t)$] expressed in terms of the radioactivity signal ratio (=(RI−BN)/(MS−BN)) by Eq. 1 (see text), X: time (min) after the start of incubation, a: slope of the line, b: intercept. Values are means±S.E.M. obtained from sixteen slices, with the exceptions of mammillary body from 8 slices.

[b] $P<0.01$; compared with the control values (Mann-Whitney U test).

[c] $P<0.01$; compared with the values of before the application of TPP.

[d] $P<0.01$; compared with the values of 20–80 min after the application of TPP (one-way ANOVA with Scheffe's post-hoc comparison test).

4. Discussion

Thiamine in its active form, TPP, is the cofactor for three enzymes involved in cerebral glucose metabolism: TK, a constituent enzyme of the pentose-phosphate pathway, and the mitochondrial enzymes PDHC and αKGDH [20,21]. Pyrithiamine is a metabolic inhibitor interfering with the synthesis of the active form TPP from thiamine [22,23]. When pyrithiamine is administered in combination with a thiamine-deficient diet, lesions resembling those of Wernicke's encephalopathy are reported to be induced with high reproducibility [5,24]. Most neurological symptoms of pyrithiamine-induced Wernicke's encephalopathy can be reversed when promptly treated with thiamine replenishment [25,26]. However, when treatment is delayed an intractable Korsakoff syndrome, the main manifestation of which is amnesic psychosis, is likely to persist, with the responsible foci having been localized to specific regions of the brain such as the thalamus and mammillary body [1,27]. Accordingly, to search for indices that identify the threshold of reversibility and its site specificity, quantitative evaluation of serial local changes in CMRglc before and after thiamine replenishment using dPAT technique is thought to be useful.

Table 2
Effect of TPP on the next influx constant of [^{18}F]FDG in the PT presymptomatic group (PT-PRE) throughout the time course (before and after the application of 1 mM TPP)[a]

Brain region		Before	20–80 min after	150–210 min after
Frontal cortex	Control	6.35±0.82	6.23±0.58	5.88±0.49
	PT-PRE	7.36±0.58	6.62±0.72	6.25±0.58
Caudate putamen	Control	7.62±0.84	6.84±0.58	6.46±0.60
	PT-PRE	7.18±0.52	6.46±0.77	6.10±0.49
Thalamus	Control	7.96±0.63	7.11±0.65	6.71±0.72
	PT-PRE	8.57±0.70	7.65±0.52	7.22±0.68
Hippocampus	Control	7.38±0.61	6.64±0.43	6.27±0.53
	PT-PRE	8.16±0.63	7.38±0.55	6.93±0.47
Mammillary body	Control	6.05±0.78	5.33±0.99	4.65±0.78
	PT-PRE	5.53±0.82	5.20±0.87	4.89±0.70
Cerebellum	Control	7.51±0.45	6.76±0.67	6.38±0.50
	PT-PRE	7.78±0.61	7.01±0.77	6.61±0.42

[a] The macroparameter $K(\times 1000)$, indicating the net influx constant of [^{18}F]FDG, was obtained from the slope of the regression Eq. ($Y=aX+b$) fitted to Patlak plots using the linear regression analysis as described in the legend of Table 1. Values are means±S.E.M. obtained from sixteen slices, with the exceptions of mammillary body from 8 slices.

The evidence for cellular viability of 300–400 μm thick fresh brain slices derives from several complementary sources reported previously [28,29]. In the present study, we considered brain slices exclusively from the aspect of metabolism, with the maintenance of a constant CMRglc used as an index of its viability. The image data obtained with dPAT were quantitatively analyzed based on Patlak graphical method [18,19]. From Eq. 1, if Cp and LC are constant, *K* and CMRglc show a proportional relation. Cp is the medium glucose concentration which at 10 mM is virtually constant, and serial assessments of *K* can be considered as an index of CMRglc assuming that LC does not change during the period from thiamine deficiency to its replenishment. After the initial part under non-steady conditions, the $Ci^*(t)/Cp^*(t)$ of the pair-fed control under unloaded normal condition showed a linear relationship with time for at least 6–7 h, with the positive slope (=net influx constant *K*) indicating the constant CMRglc during this time course.

Prior to TPP administration, in the PT symptomatic group as compared to the pair-fed control group *K* value increased in all regions with the exception of the thalamus and mammillary body. So far, a study on local cerebral glucose utilization (LCGU) using [^{14}C]2DG quantitative autoradiographic technique [30] demonstrated that pyrithiamine treatment in the rat resulted in a paradoxical increase in LCGU in several regions of the brain just prior to the onset of neurological symptoms. The most likely explanation for this increase in LCGU was surmised to be increased glycolysis resulting from a metabolic adaptation as a consequence of decreased αKGDH activity primarily [30,31] and aimed at maintaining ATP levels by anaerobic means [32]. In the present study with TPP administration as the trigger *K* value in all sites showed a dramatic decrease, proving that prior to TPP administration a transient compensation was induced by this kind of anaerobic glycolysis. Namely, as the underlying biochemical mechanism, it is surmised that the TPP supplementation led to activated pyruvate oxidation into the citric acid cycle with the hitherto accumulated lactate as the substrate, accompanying which the enhanced glycolysis was inhibited. This was proved by the fact that lactate concentrations in the slices decreased in a temporally consistent fashion with reductions in the net influx constant of [^{18}F]FDG immediately after TPP administration. Lactate has been considered for many years to be a useless, and frequently, harmful end-product. Schurr et al. [33] showed that lactate, as a sole energy substrate, can support neuronal function in hippocampal slice preparations, which finding was later reproduced by others. Furthermore, by quantitatively evaluating the dynamic changes in the [^{18}F]FDG uptake by lactate loading using the same dPAT as in the present study, we demonstrated the preference of lactate over glucose as an energy substrate in normal brain tissue under normoxic condition [34]. On the other hand, in the pair-fed control, the lactate concentration within the brain slices showed no change either before or after TPP-loading with an almost constant *K* value shown throughout. In the slices immersed in the incubation solution in the present dPAT experimental system, all incubation conditions before and after TPP administration were consistent with the exception of the addition of TPP to the bathing medium. Accordingly, the changes in the K values and lactate concentration before and after TPP-loading in the PT symptomatic group in the present study are thought to reflect the specific changes in glucose metabolism in brain tissue induced by the correction of thiamine deficiency.

Hakim and Pappius [30] have pointed out that the above-mentioned increase in [^{14}C]2DG uptake rate immediately prior to the expression of the neurological symptoms was observed primarily in the thalamus. Instead, the net influx constant of [^{18}F]FDG in the present PT presymptomatic group did not differ from that of the control group at any site either before or after TPP administration. Further studies on the mechanisms underlying these contradictory results are being awaited. If in the present study the period just prior to the onset of neurological symptoms had been more accurately pinpointed by painstaking observation of behavior and other means, it might have been possible to specify the period when the net influx constant of [^{18}F]FDG increased in the thalamus as well. Conversely, in the PT symptomatic group, the net influx constant in the thalamus and mammillary body was markedly decreased, both considered to be representative sites of selective damage responsible for Korsakoff syndrome [1,27]. The decreased net influx constant of [^{18}F]FDG in these sites did not show any recovery at all even more than 150 min after TPP-loading, possibly reflecting the irreversible neurological damage that develops once the stage of mere biochemical functional abnormality induced by thiamine deficiency is exceeded. In contrast, in the other sites despite some degree of difference recovery to close to the values of the pair-fed control group was observed. Accordingly, site differences in the degree of recovery of CMRglc after TPP administration may well be related to the localized foci responsible for Korsakoff syndrome which responds poorly to thiamine therapy.

In conclusion, the present findings suggest that use of dPAT technique to quantitatively evaluate serial local changes in CMRglc from thiamine deficiency to after its replenishment may be useful in elucidating the pathophysiology and prognosis of Wernicke's encephalopathy.

Acknowledgements

This study was supported in part by the research Grant (JSPS-RFTF97L00203) for 'Research for the Future' Program from the Japan Society for the Promotion of Science.

References

[1] Victor M, Adams RD, Collins GH, editors. Contemporary neurology series, The Wernicke-Korsakoff syndrome, Vol. 7, FA Davis, Philadelphia, 1971, pp. 36–45.

[2] Harper CG. The incidence of Wernicke's encephalopathy in Australia: a neuropathological study of 131 cases. J Neurol Neurosurg Psychiat 1983;46:593–8.

[3] Yokote K, Miyagi K, Kuzuhara S, Yamanouchi H, Yamada H. Wernicke encephalopathy: follow-up study by CT and MR. J Comput Assist Tomogr 1991;15:835–8.

[4] Troncoso JC, Johnson MV, Hess KM, Griffin JW, Price DL. Model of Wernicke's encephalopathy. Arch Neurol 1981;38:350–4.

[5] Leong DK, Le O, Oliva L, Butterworth RF. Increased densities of binding sites for the 'peripheral-type' benzodiazepine receptor ligand [^{3}H]PK11195 in vulnerable regions of the rat brain in thiamine deficiency encephalopathy. J Cereb Blood Flow Metab 1994;14:100–5.

[6] Hollowach J, Kauffman F, Ikossi Maria G, Thomas C, McDougal DGJ. The effects of a thiamine antagonist, pyrithiamine, on levels of selected metabolic intermediates and on activities of thiamine-dependent enzymes in brain and liver. J Neurochem 1968;15:621–31.

[7] Gaitonde MK, Fayein NA. Decreased metabolism in vivo of glucose into amino acids of the brain of thiamine-deficient rats after treatment with pyrithiamine. J Neurochem 1975;24:1215–23.

[8] Cole M, Turner A, Frank O, Baker H, Leevy CM. Extra-ocular palsy and thiamine therapy in Wernicke's encephalopathy. Am J Clin Nutr 1969;22:44–51.

[9] Bonjour JP. Vitamins and alcoholism. Int J Vitam Nutr Res 1980;50:321–38.

[10] Feinberg JF. The Wernicke-Korsakoff syndrome. Am Fam Physician 1980;22:129–33.

[11] Sokoloff L, Reivich M, Kennedy C, Des Rosiers MH, Patlak CS, Pettigrew KD, Sakurada O, Shinohara M. The [^{14}C]deoxyglucose method for the measurement of local cerebral glucose utilization: theory, procedure, and normal values in the conscious and anesthetized albino rat. J Neurochem 1977;28:897–916.

[12] Newman GC, Hospod FE, Patlak CS. Brain slice glucose utilization. J Neurochem 1988;51:1783–96.

[13] Matsumura K, Bergström M, Onoe H, Takechi H, Westerberg G, Antoni G, Bjurling P, Jacobson GB, Långström B, Watanabe Y. In vitro positron emission tomography (PET): use of positron emission tracers in functional imaging in living brain slices. Neurosci Res 1995;22:219–29.

[14] Murata T, Matsumura K, Onoe H, Bergström M, Takechi H, Sihver S, Sihver W, Neu H, Andersson Y, Ögren M, Fasth KJ, Långström B, Watanabe Y. Receptor imaging technique with ^{11}C-labeled receptor ligands in living brain slices: its application to time-resolved imaging and saturation analysis of benzodiazepine receptor using [^{11}C]Ro15-1788. Neurosci Res 1996;25:145–54.

[15] Hamacher K, Coenen HH, Stocklin G. Efficient stereospecific synthesis of no-carrier-added 2-[F-18]-fluoro-2-deoxy-D-glucose using aminopolyether supported nucleophilic substitution. J Nucl Med 1986;27:235–8.

[16] Huang SC, Phelps ME, Hoffman EJ, Sideris K, Selin CJ, Kuhl DC. Noninvasive determination of local cerebral metabolic rate of glucose in man. Am J Physiol 1980;128:E69–82.

[17] Phelps ME, Huang SC, Hoffman EJ, Slein C, Sokoloff L, Kuhl DE. Tomographic measurement of local cerebral glucose metabolic rate in humans with (F-18)2-fluoro-2-deoxy-D-glucose: validation of method. Ann Neurol 1979;6:371–88.

[18] Patlak CS, Blasberg RG, Fenstermacher JD. Graphical evaluation of blood-to-brain transfer constants from multiple-time uptake data. J Cereb Blood Flow Metab 1983;3:1–7.

[19] Patlak CS, Blasberg RG. Graphical evaluation of blood-to-brain transfer constants from multiple-time uptake data. Generalizations. J Cereb Blood Flow Metab 1985;5:584–90.

[20] Butterworth RF. Effect of thiamine deficiency on brain metabolism: implications for the pathogenesis of the Wernicke-Korsakoff syndrome. Alcohol and Alcoholism 1989;24:271–9.

[21] Leong DK, Butterworth RF. Neuronal cell death in Wernicke's encephalopathy: pathophysiologic mechanisms and implications for PET imaging. Metab Brain Dis 1996;11:71–9.

[22] Rindi G, Perri V. Uptake of pyrithiamine by tissue of rats. Biochem J 1961;80:214–6.

[23] Heroux M, Butterworth RF. Regional alterations of thiamine phosphate esters and of thiamine-diphosphate-dependent enzymes in relation to function in experimental Wernicke's encephalopathy. Neurochem Res 1995;20:87–93.

[24] Watanabe I. Pyrithiamine-induced acute thiamine-deficient encephalopathy in the mouse. Exp Mol Pathol 1978;28:381–94.

[25] Hakim AM, Carpenter S, Pappius HM. Metabolic and histological reversibility of thiamine deficiency. J Cereb Blood Flow Metab 1983;3:468–77.

[26] Butterworth RF, Heroux M. Effect of pyrithiamine treatment and subsequent thiamine rehabilitation on regional cerebral amino acids and thiamine dependent enzymes. J Neurochem 1989;82:1079–84.

[27] Mair RG, Knoth RL, Rabchenuk SA, Langlais PJ. Impairment of olfactory, auditory, and spatial serial reversal learning in rats recovered from pyrithiamine-induced thiamine deficiency. Behav Neurosci 1991;105:360–74.

[28] Van Huizen F, Shaw C, Wilkinson M, Cynader M. Characterization of muscarinic acetylcholine receptors in rat cerebral cortex with concomitant morphological and physiological assessment of tissue viability. Mol Brain Res 1989;5:59–69.

[29] Shaw CA, Wilkinson M. Receptor characterization and regulation in intact tissue preparations. Pharmacological implications. Biochem Pharmacol 1994;47:1109–19.

[30] Hakim AM, Pappius HM. Sequence of metabolic, clinical, and histological events in experimental thiamine deficiency. Ann Neurol 1983;13:365–75.

[31] Butterworth RF, Giguere JF, Besnard AM. Activities of thiamine-dependent enzymes in two experimental models of thiamine-deficiency encephalopathy 2. Alpha-ketoglutarate dehydrogenase. Neurochem Res 1986;11:567–77.

[32] Parker WDJ, Haas R, Stumpf DA, Parks J, Eguren LA, Jackson C. Brain mitochondrial metabolism in experimental thiamine deficiency. Neurology 1984;34:1477–81.

[33] Schurr A, West CA, Rigor BM. Lactate-supported synaptic function in the rat hippocampal slice preparation. Science 1988;240:1326–8.

[34] Murata T, Waki A, Omata N, Fujibayashi Y, Sadato N, Yano R, Yoshimoto M, Isaki K, Yonekura Y. Dynamic changes in glucose metabolism by lactate loading as revealed by a positron autoradiography technique using rat living brain slices. Neurosci Lett 1998;249:155–8.